Int. J. Electrochem. Sci., 17 **(2022)** Article Number: 221286, doi: 10.20964/2022.12.77

International Journal of
ELECTROCHEMICAL
SCIENCE
www.electrochemsci.org

Numerical Study of Aluminum Pitting Corrosion Using a Two-Dimensional Multi-Species Transport Model

Meriyem Mouloudi[1,], Mohamed Essahli[1], Mostafa Chhiba[2] and Mohammed Chafi[3]*

[1] Laboratory of Applied Chemistry and Environment, Faculty of Sciences and Techniques, Hassan First University, BP 577, Settat, Morocco
[2] Radiations materials & instrumentations Laboratory, Faculty of Sciences and Techniques, Hassan First University, BP 577, Settat, Morocco
[3] Laboratory of Chemical Engineering and Environment, Higher School of Technology, Hassan II University, BP 8012, Oasis Casablanca, Morocco
[*]E-mail: meriyem.mouloudi@gmail.com

Received: 6 October 2022 / *Accepted:* 23 November 2022 / *Published:* 27 December 2022

Pitting corrosion is a local degradation of the passivation layer formed on the metal surface. It is considered more dangerous than uniform corrosion because the cavities fill with corrosion products and are thus difficult to detect. Considering the complexity of the phenomena involved in the pitting corrosion process, numerical simulation based on the finite element method is a timely tool to overcome the difficulties and limitations of experimental studies. In this study, a two-dimensional numerical model has been developed to simulate the behavior of aluminum against pitting corrosion in a sodium chloride solution. This simulation is based on the resolution of the Nernst-Planck equation describing the mass transport phenomena and the reactions of chemical species in solution. The results show that the local chemistry of the pit has an effect on the evolution of pitting corrosion. Furthermore, the pit geometrical shape influences the corrosion behavior due to the role of the local chemistry in solution and the electric field at the metal/solution interface.

Keywords: Aluminum; pitting corrosion; Nernst-Planck equation; finite element method; numerical simulation.

1. INTRODUCTION

Corrosion is defined as a physico-chemical reaction between a metal and its environment (aqueous or gaseous) that leads to changes in the properties of the metal and in particular a significant degradation of its function [1,2]. Crevice, uniform and pitting corrosion and others are various forms of corrosion of metallic materials likely to occur in an aqueous environment. Several factors related to the

intrinsic characteristics, the conditions of use and the exposure environment of the metal, impact the form of corrosion developed [1].

Despite the best corrosion resistance of aluminum, it is susceptible to pitting corrosion, which occurs through local degradation of the passivation layer formed on the surface of the metal in sufficiently aggressive environments containing chlorides, bromides, iodides or perchlorates [3]. The pitting attack can reach a depth of the order of a millimeter but generally does not exceed several tens to a few hundred micrometers in diameter while the rest of the surface remains intact [1]. According to the literature [4,5], pitting can have narrow and deep, hemispherical or shallow and wide shapes.

The pitting corrosion process starts with a local rupture of the passive layer which propagates as holes in the material giving rise to the cavities. Previous work [6-8] has shown that this process goes through three stages: (1) metal-solution interaction and rupture of the passive film; (2) formation of metastable pits; and (3) stable growth of the pits.

The kinetics of the electrodes and the local environment of the pits are generally controlled by the electrochemical and chemical reactions involved in the growth of the pits as well as by the process of mass transport [9]. The finite element method on which the numerical simulation is based is an appropriate tool to predict the evolution of the pitting corrosion in a given environment by using the resolution of the transport/reaction equations.

Recent studies have focused on the numerical simulation of pitting corrosion by including the mass transport processes and the electrochemical kinetics in the electrolyte.

In 2011, a numerical model by the finite element method (FEM) was performed by Oltra *et al.* [10] for the calculation of the dissolution rate of aluminum in an alkaline medium assuming a pH-dependent kinetic law, and the obtained results prove that chemistry controls the initiation of aluminum dissolution. On the other hand, Xiao & Chaudhuri [11] presented a FEM numerical model of pitting corrosion of aluminum alloys and found that through numerical simulation, we can quantitatively correlate the corrosion rate with the environment inside the pit which is difficult to obtain from experiments, and furthermore to many key factors namely the microstructure and composition of the alloy, the solution chemistry, the applied potential and the pitting geometry.

Furthermore, Salleh & Stevens [3,12,13] have developed numerous mathematical models of pitting corrosion propagation on steel considering both electrochemical and chemical reactions. The Nernst-Planck equation has been used to solve the models proposed by the authors and the results obtained allow to illustrate the current densities, the pH within the pit and the ionic species concentrations.

In addition, Guseva *et al.* [14,15] presented two mathematical models including only chemical reactions in the electrolyte. The first model deals with the anodic dissolution of aluminum in a sodium chloride solution while the second one studies the temporal evolution of the local chemical environment of the localized corrosion in aluminum alloys during the initial phase. The results obtained confirm a difference in species concentrations between the temporal and stationary modes of calculation and that current densities exceeding 0.1 A/cm^2 can be identified as active dissolution because they significantly affect the potential values and species concentrations.

Also, Wang *et al.* [16] studied the evolution of localized corrosion as a function of time in natural gas and oil pipelines by numerical simulation considering various chemical and electrochemical

reactions at the electrode/solution interface. A good correlation between the local chemical environment and electrical conditions in the pit was concluded from the results found by Wang *et al.* [16].

Moreover, Mouloudi *et al.* [17] in 2021 suggested an aluminum pitting corrosion model based on the Laplace equation. The objective was to demonstrate the effect of the electrolyte and the influence of the geometry on pitting growth by illustrating the potential and current distribution. However, this study only examined the electrochemical phenomena involved in the pitting corrosion process.

In the present work, we have developed a two-dimensional model of aluminum pitting corrosion by coupling electrochemical processes to the transport of different species. The diffusion and migration transport equations were solved using the finite element software COMSOL Multiphysics.

The objective is to study by numerical simulation the behavior of aluminum against pitting corrosion in a 1M NaCl solution while examining the ion concentration, the pH distribution and the kinetics of the electrochemical process.

2. MATERIAL AND METHOD

In this paper, the approach chosen is based on the numerical simulation of pitting corrosion by the finite element method (FEM). This simulation is based on a modeling of the mass transport processes as well as a set of chemical reactions in the solution and electrochemical reactions at the electrode/solution interface. The model developed during this study takes into account:

- An approximated geometry of the studied pit shape;
- Mass transport by diffusion and migration within an electrically neutral electrolyte;
- Chemical reactions in the electrolyte at equilibrium;
- Electrochemical reactions (oxidation and reduction) taking place at the surface pitting.

2.1. Governing equations

Mass transport in the electrolyte occurs by diffusion and migration and the convection term has been neglected in this work.

The flux equation called the Nernst-Planck equation translating the conservation of mass for each species *i* in the media, is written as follows [10,16,18-20] :

$$N_i = -D_i \nabla C_i - z_i u_i F C_i \nabla \phi \quad (1)$$

With C_i is the concentration of species i, ϕ the electrostatic potential in solution, $N_i$is the flux of species i, F is the Faraday constant, D_i is the diffusion coefficient of species i, z_i is the charge of species i, $u_i$is the mobility of species i given by the following Nernst-Einstein equation [18]:

$$u_i = \frac{D_i}{RT} \quad (2)$$

The mass balance for a species i in solution is given by the following relation [18,19]:

$$\frac{\partial C_i}{\partial t} + \nabla N_i = R_i \quad (3)$$

Where R_i denotes the reaction rate or production/consumption term of species i within the volume.

The Nernst-Planck equation is solved for each species considered in the model. Since the potential is unknown, another equation of state is required to determine it.

The potential can be solved by the following Poisson's equation [18]:

$$\nabla^2\phi = -\frac{\mathrm{F}}{\varepsilon}\sum_{\mathrm{i}} z_i C_i \quad (4)$$

In aqueous solution at 25 °C, the ratio F / ε is > 1 which imposes the electroneutrality relation.

As found by Sharland *et al.* [21], the Poisson's equation is replaced by the local charge neutrality equation presented as follows [18,19]:

$$\sum_i z_i C_i = 0 \quad (5)$$

2.2. Description of the model

2.2.1. Electrochemical reactions

In the present work, we considered two electrochemical reactions at the metal surface. These are the oxidation of aluminum and the reduction of the proton [12,22] :

$$Al \rightarrow Al^{3+} + 3e^- \quad (6)$$

$$2H^+ + 2e^- \rightarrow H_2 \quad (7)$$

The rate laws for these electrochemical reactions are expressed from the experimentally determined Butler-Volmer equations. The current densities for aluminum oxidation and proton reduction are respectively given by Oltra *et al.* [10]:

$$i_{Al} = i_{Al}^0 \, e\exp\left(\frac{(V_m - \phi - E_{Al}^0)}{b_{Al}}\right) \quad (8)$$

$$i_{H^+} = -2Fk_{H^+}C_{H^+} \exp\left(-\frac{\left(V_m - \phi - E_{H^+}^0\right)}{b_{H+}}\right) \quad (9)$$

i_{Al} and i_{H+} are respectively the current densities of aluminum oxidation and proton reduction, i_{Al}^{0} and i_{H+}^{0} correspond to the current densities at equilibrium, b_{Al} and b_{H+} are the Tafel coefficients, C_{H+} is the proton concentration, F is the Faraday constant, k_{H^+} is the interfacial rate constant, E is the electrode potential which is defined by the difference in electrical potential between the metal V_m and the electrolyte ϕ.

A standard hydrogen electrode is used as the reference electrode. The parameters of the electrochemical reactions are presented in Table 1:

Table 1. Electrochemical reactions and their kinetic parameters [10,23]

Electrochemical Reactions	Parameters
$\boldsymbol{Al \rightarrow Al^{3+} + 3e^{-}}$	E_{Al}= -1.352 V_{SCE} i_{Al}= 2.12 µA/cm^2 b_{Al}= 0.25 V
$\boldsymbol{2H^{+} + 2e^{-} \rightarrow H_2}$	E_{H+}= -1 V_{SCE} k_{H+}= 10^{-5} m/s b_{H+}= 0.05 V

2.2.2. Chemical reactions

For any homogeneous chemical reaction between the species A_i present in solution:

$$\sum_{i} v_{A_i} A_i \underset{k_{ib}}{\overset{k_{if}}{\rightleftarrows}} \sum_{i} v_{B_i} B_i \tag{10}$$

The reaction rate R_i or production/consumption term is expressed as follows:

$$R_i = k_{if} \prod_{i} C_{A_i}^{v_{A_i}} - k_{ib} \prod_{i} C_{B_i}^{v_{B_i}} \tag{11}$$

The chemical reactions considered in this model are presented as follows:

$$H_2O \underset{k_b}{\overset{k_f}{\rightleftarrows}} H^+ + OH^- \tag{12}$$

$$Al^{3+} + H_2O \underset{k_b}{\overset{k_f}{\rightleftarrows}} AlOH^{2+} + H^+ \tag{13}$$

The expressions R_i corresponding to the autoprotolysis of water and the hydrolysis of metal cations Al^{3+} are respectively given below:

$$R_{H^+} = k_f c_{H_2O} - k_b c_{H^+} c_{OH^-} \quad (14)$$

$$R_{AlOH^{2+}} = k_f c_{Al^{3+}} - k_b c_{AlOH^{2+}} c_{H^+} \quad (15)$$

According to the theory of dilute solutions, we consider that the chemical reactions are at equilibrium ($K = \frac{k_f}{k_b}$). Table 2 shows the corresponding equilibrium constants at 25°C:

Table 2. Chemical reactions and their respective equilibrium constants [5,15]

Chemical Reactions	**Kinetic constant in forward direction k_f**	**Kinetic constant in backward direction k_b**
$\boldsymbol{Al^{3+} + H_2O \rightarrow AlOH^{2+} + H^+}$	1.09×10^{5} s^{-1}	4.4×10^{9} $M^{-1}s^{-1}$
$\boldsymbol{H_2O \rightarrow H^+ + OH^-}$	2.06×10^{-5} s^{-1}	1.3×10^{11} $M^{-1}s^{-1}$

In this study, a sodium chloride NaCl solution of 1M concentration with pH 6 was used as electrolyte. The present model consists of six species: OH^-, H^+, Al^{3+}, $AlOH^{2+}$, Na^+ and Cl^-. However, Na^+ sodium ions are not involved in the pitting corrosion process but they help to maintain electroneutrality at the pit mouth. Table 3 summarizes the constants used in this study for these six chemical species.

Table 3. Charge number z_i, diffusion coefficients D_i, initial concentration C_{i0}, of chemical species [5,15]

Species	$\boldsymbol{z_i}$	$\boldsymbol{D_i}$ **($\times10^{-9}$ m^2s^{-1})**	$\boldsymbol{C_{i0}}$ **(mol dm^{-3})**
Na^+	1	1.334	1
Cl^-	-1	2.032	1
H^+	1	9.311	10^{-6}
OH^-	-1	5.273	10^{-8}
Al^{3+}	3	0.541	0
$AlOH^{2+}$	2	0.541	0

2.2.3. Geometry and Boundary Conditions

An approximate two-dimensional 2D geometry of a hemispherical shaped pitting was chosen to numerically simulate the pitting corrosion behavior of aluminum. Figure 1 shows the model geometry used where the pit radius R_{pit} is 50 µm with a thin layer of electrolyte solution with a thickness of 200 µm.

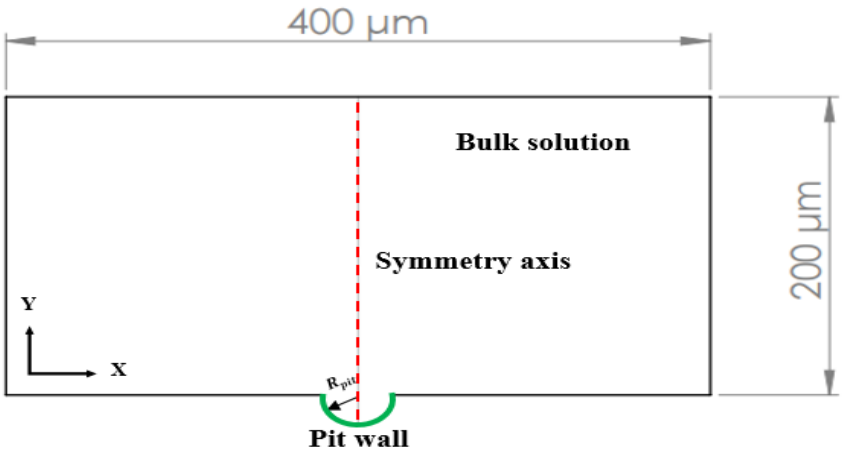

Figure 1. Axisymmetric geometry of the pit in 2D.

For the reactive boundaries, we express the total current density i_{tot} sum of the anodic and cathodic current densities [24]:

$$i_{tot} = \sum_k i_{A_k} \tag{16}$$

Where i_{A_k} is the current density associated with each electrochemical reaction. The flux N_{A_k} of each species A_k involved in an electrochemical reaction is written as follows (Neumann condition) [8,24] :

$$\text{n}.N_{A_k} = \frac{v_k}{v_e F} i_{A_k} \tag{17}$$

With n is the normal vector of the boundary directed towards the interior of the domain, v_k is the stoichiometric coefficient of the species A_k and v_e is the number of electrons involved in the electrochemical reaction.

The other boundaries delimiting the subdomain in which the Nernst-Planck equation has been solved have been considered insulating. Thus the boundary condition is expressed by the following relation [8,24]:

$$\mathrm{n}.N_{A_k} = 0 \tag{18}$$

In this case, the flux of each species is zero and an electrical isolation condition is imposed for the current:

$$i_{A_k} = 0 \tag{19}$$

The boundary conditions at the boundaries imposed in this model are shown in Figure 2:

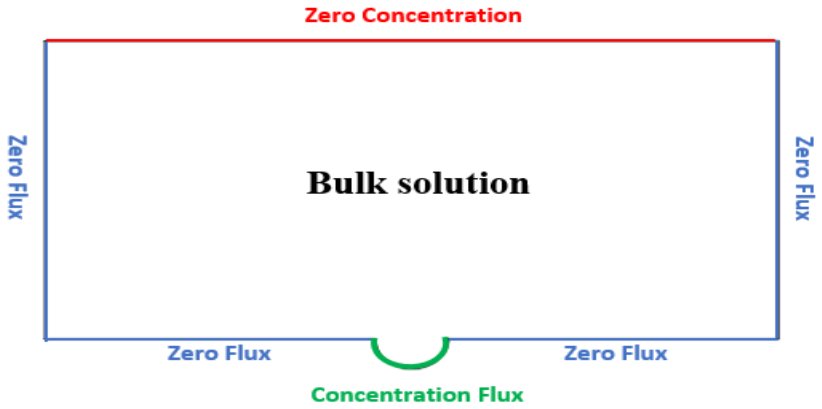

Figure 2. Boundary conditions at the model boundaries.

The present study was performed at a temperature of 298.15 K in the absence of the film.

3. RESULTS AND DISCUSSION

The governing equations, boundary conditions and mesh were applied to the geometry described in Figure 1, incorporating the electrochemical and chemical phenomena considered in this study. The results obtained are presented and discussed below.

3.1. Evolution dynamics of pitting corrosion

Solving the Nernst-Planck equation allows us to present the concentration distribution of Al^{3+}, H^{+} and $AlOH^{2+}$ ions on the pit surface. The results found are presented in Figure 3.

We can see from Figure 3a that the concentration distribution of Al^{3+} is higher inside the pit than on the sidewalls due to the anodic dissolution of aluminum.

The positively charged Al^{3+} ions are balanced by the migration of negatively charged chloride ions Cl^- to the bottom of the pit, which is consistent with the studies of Salleh & Stevens [3,12,13] who confirmed that the environment inside the pit is positively charged due to the dissolution of the metal which attracts chloride ions through the migration process to maintain electroneutrality. The increase in the concentration of Cl^- ions results in a negatively charged medium in the pit and consequently attracts the H^+ ions produced by the water dissociation reaction.

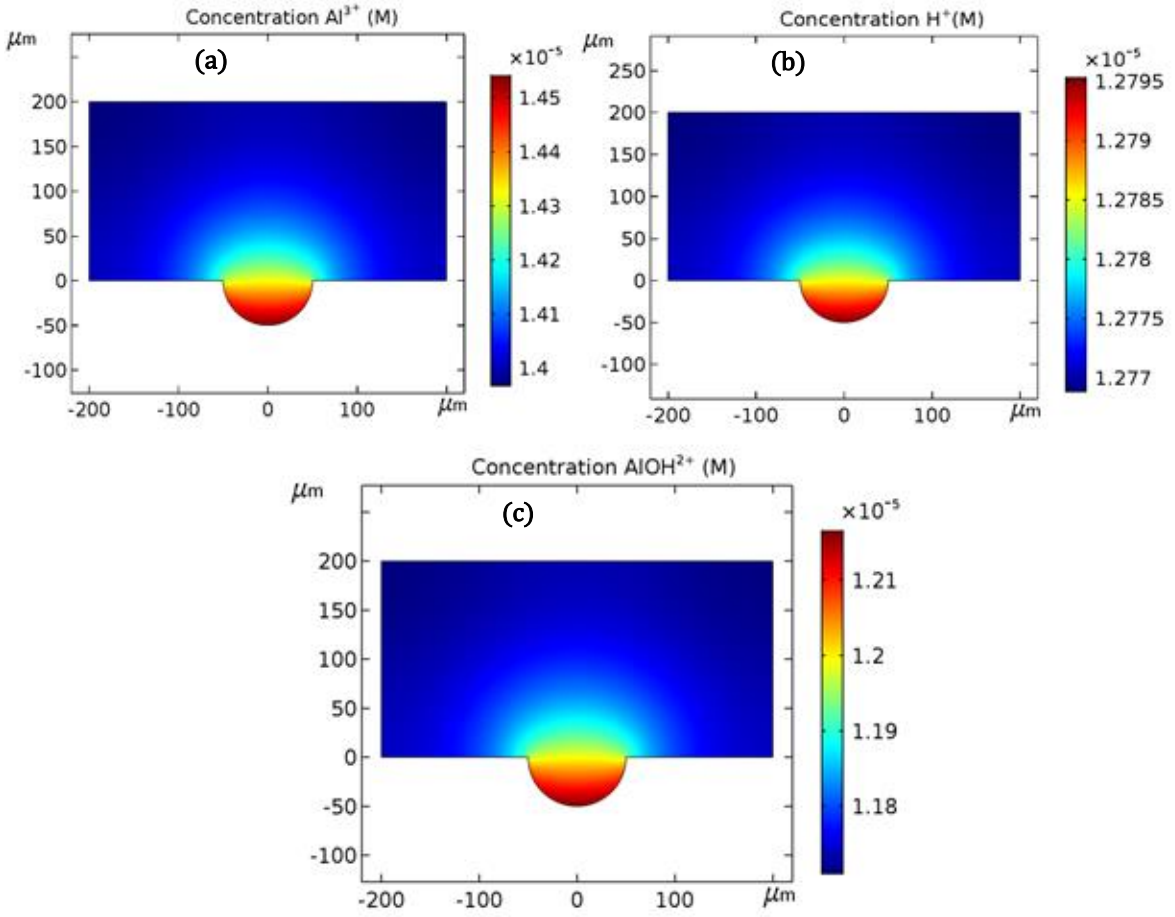

Figure 3. Concentration distribution at 3600s: (a) Al^{3+}; (b) H^+; (c) $AlOH^{2+}$.

The H^+ concentration distribution shown in Figure 3b indicates the accumulation of H^+ at the bottom of the pit. The presence of H^+ and Cl^- ions leading to an acidic and corrosive environment promotes metal dissolution. These results are in good agreement with the work of Xiao & Chaudhuri [11], Lee *et al.* [25] and Yuan *et al.* [26].

In addition, the high concentration of Al^{3+} promotes the hydrolysis reaction in the presence of water which produces the $AlOH^{2+}$ ions shown in Figure 3c and consequently the abundance of H^+ ions reduces the pH at the bottom of the pit as proven by Sato [27].

The pH is expressed by the following equation:

$$pH = -log_{10}[H^+] \quad (20)$$

From the above equation, we can see that the pH is low at the bottom of the pit compared to the electrolyte solution. Therefore, it is mainly the hydrolysis reaction that controls the pH in the pit as has been confirmed by Salleh & Stevens [3,12,13], Lee *et al.* [25] and Tricoit [28].

The acidic environment favors metal dissolution at the active sites (bottom/mouth of the pit) and this process evolves as a function of exposure time. The expression of the corrosion rate at the pit interface is calculated on the basis of the Faraday law according to the following equation [17]:

$$C_R = \frac{I_{corr} \times M_{Al}}{\mathrm{z} \times \mathrm{F} \times \rho_{Al}} \quad (21)$$

Where C_R is the corrosion rate, I_{corr} is the corrosion current density (A/m^2), M_{Al} and ρ_{Al} are the molar mass and density of aluminum respectively with M_{Al} =0.02698 kg/mol and ρ_{Al} = 2700 kg/m^3, z is the aluminum valence z = 3 and F is the Faraday constant F = 96500 A·s/mol.

The corrosion rate C_R is plotted as a function of time at the active sites that are at the bottom and mouth of the pit.

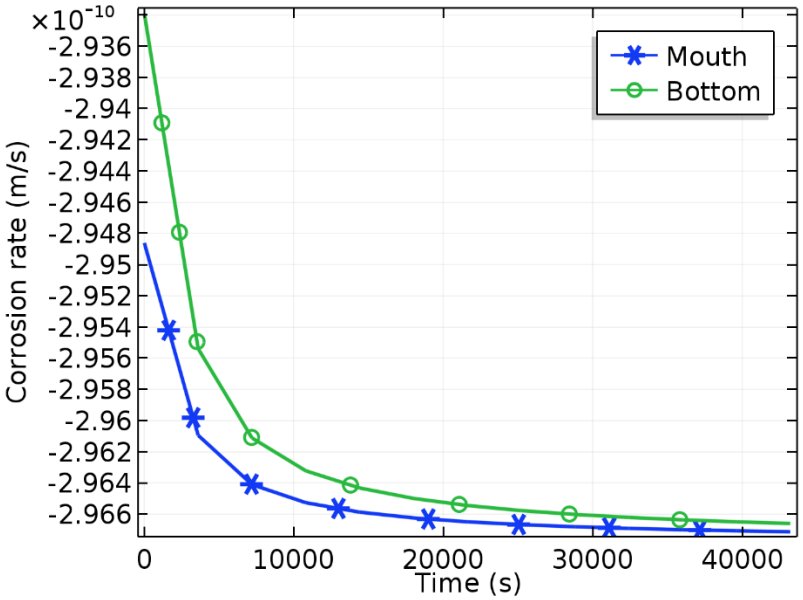

Figure 4. Corrosion rate at bottom and mouth of pit.

According to Figure 4, we notice that the corrosion rate increases progressively as a function of time and that this rate is higher at the mouth than at the bottom of the pit as confirmed by Mouloudi *et*

al. [17]. The difference in the corrosion rate between the bottom and the mouth of the pit is due to the formation of rust or aluminum oxide that prevents the further dissolution of the metal according to the work of Salleh & Stevens [12].

3.2. Effect of the pit shape on the evolution of the pitting corrosion

The ion concentration distribution and the electric field within the pit can be influenced by the pit shape. In order to understand how the geometric shape affects the pitting corrosion behavior, we modified the initial geometry shown in Figure 1. The Al^{3+} concentration distribution for hemispherical pit, deep pit and shallow pit is shown in Figure 5:

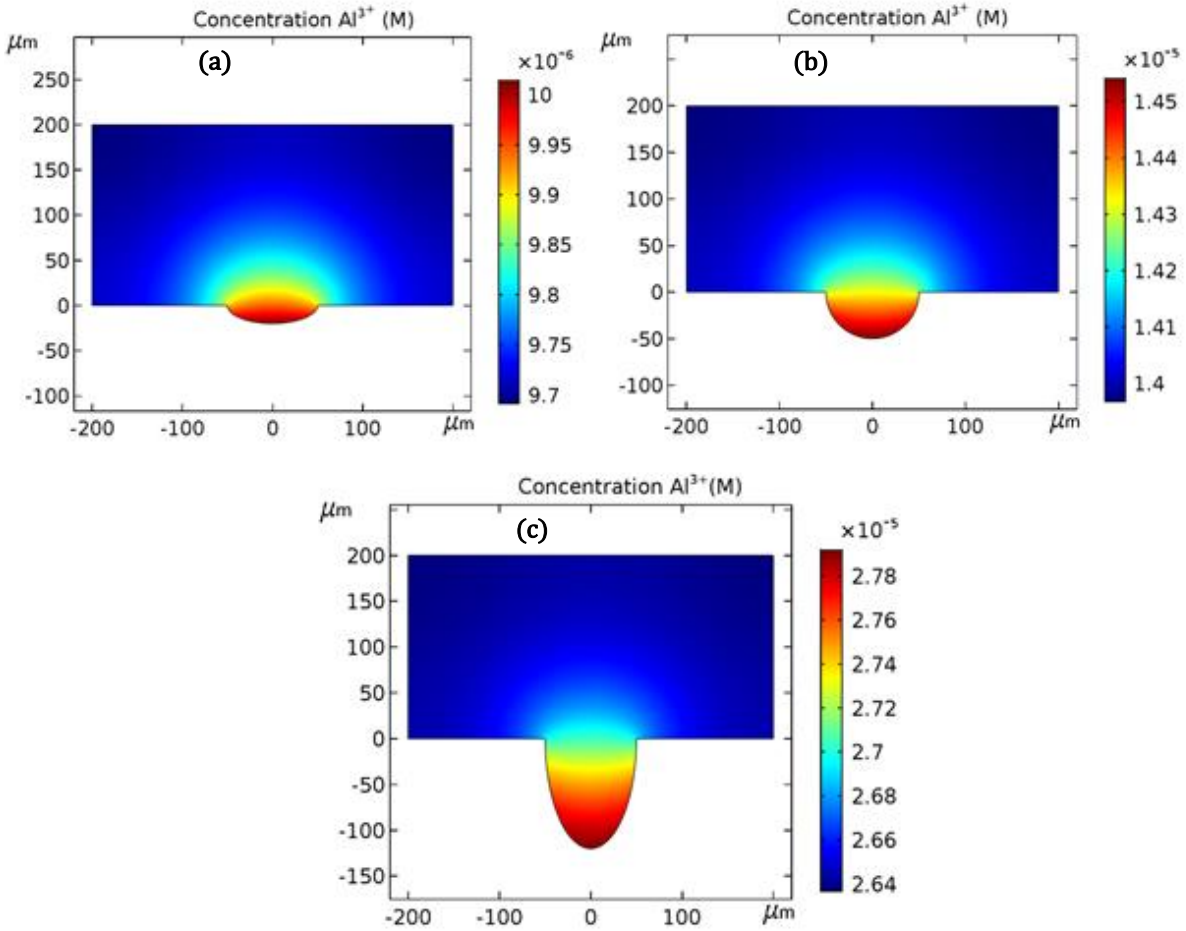

Figure 5. Al^{3+} concentration distribution for different pit shapes: (a) Shallow pit; (b) Hemispheric pit; (c) Deep pit.

From Figure 5c, it can be clearly seen that the concentration in the deep pit is higher and the mass transport at the bottom of the pit to the bulk solution is more difficult which facilitates the accumulation of Al^{3+}. On the other hand, the mass transport for the shallow pit is easier outward through the mouth of the pit and therefore the concentration of Al^{3+} in the pit is low according to Figure 5a. Furthermore,

Figure 5b shows that the Al^{3+} concentration for the hemispherical pit is between the deep pit and the shallow pit.

Due to the hydrolysis of $Al^{3+,}$ the concentration of H^+ accumulates in abundance inside pit which leads to a corrosive environment. Figure 6 represents the influence of the pit shape on the H^+ concentration.

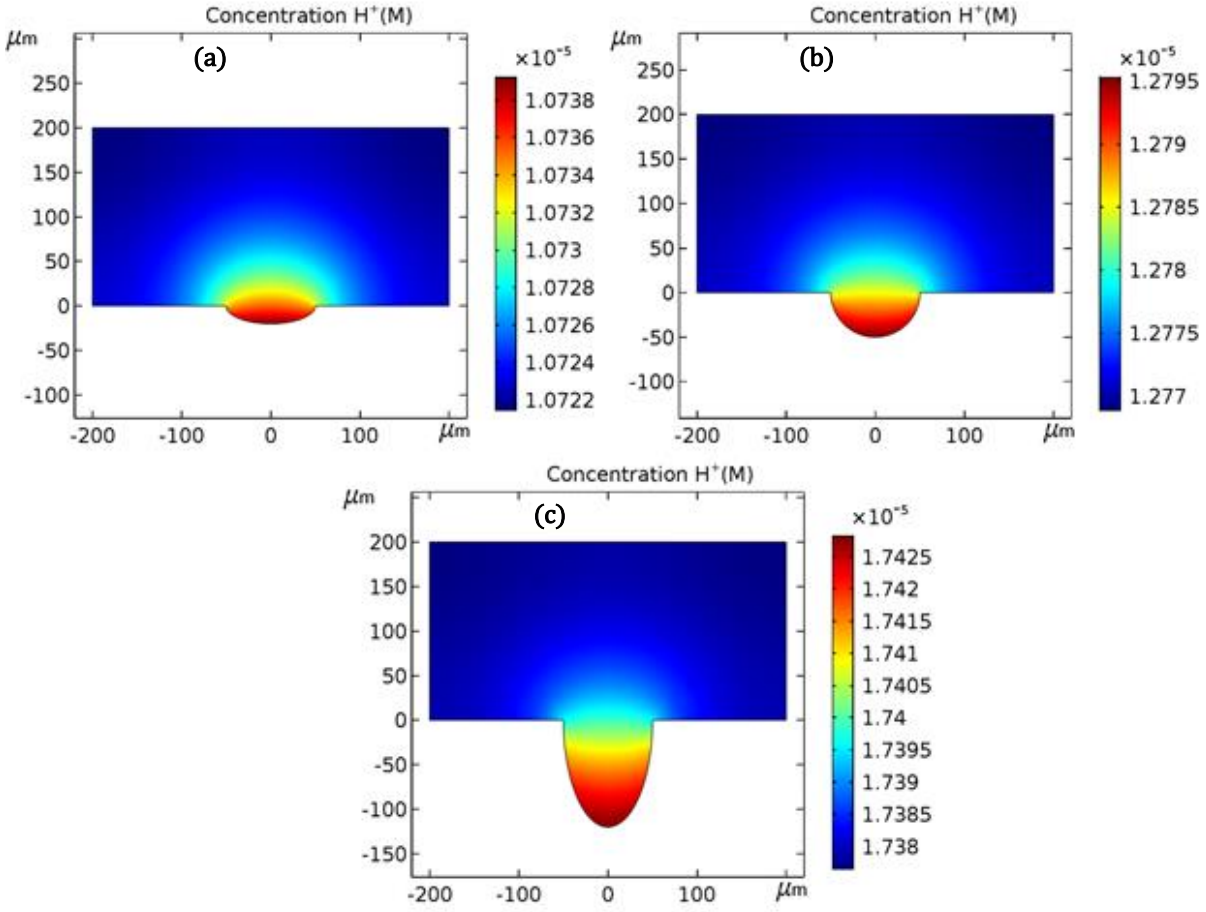

Figure 6. Influence of the pit shape on the concentration distribution of H^+: (a) Shallow pit; (b) Hemispheric pit; (c) Deep pit.

The concentration of H^+ in the deep pit is higher than the hemispheric pit and the shallow pit as shown in Figure 6. This is due to the high concentration of Al^{3+} in the deep pit which promotes the hydrolysis reaction and thus the abundance of H^+ ions which reduces the pH.

These findings are in agreement with the results in the literature by Wang *et al.* [16] and Tricoit [28] who confirmed that the pit shape has an influence on the local chemical and electrical environment in the pit. The current density along the pit wall for different geometric shapes is shown in Figure 7.

We see from Figure 7 that the electrolyte current density is slightly higher in the deep pit compared to the other pit forms due to the high concentration of H^+. Furthermore, it can be seen that the current density profiles move in the same direction as the Al^{3+} and H^+ ion concentration profiles for the

three geometric shapes studied. In summary, the ion concentration distribution has an effect on the electrolyte current density profiles.

Furthermore, for a given geometric shape, we find a current density difference between the bottom and the mouth of the pit. This difference is even more important when the depth of the pit is high, which has been proved by Tricoit [28] and Mouloudi *et al.* [17].

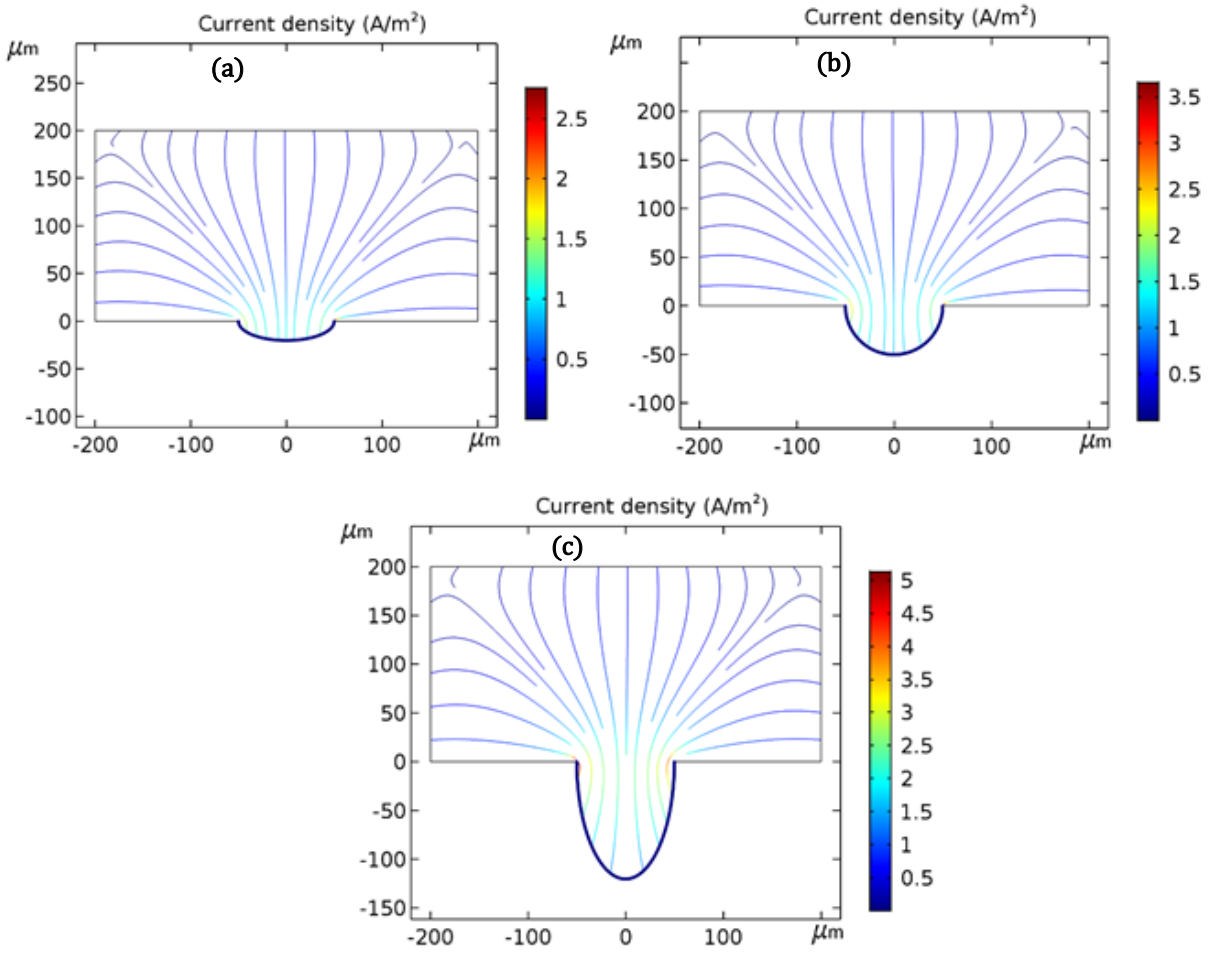

Figure 7. Influence of pit shape on electrolyte current density along the pit wall: (a) Shallow pit; (b) Hemispherical pit; (c) Deep pit.

According to previous work by Tricoit [28] and Mouloudi *et al*. [17], the deeper the pitting, the greater the ohmic drop in potential, which leads to differences in the corrosion rate between the bottom and the mouth of the pit and consequently the corrosion rate C_R along the metal wall decreases when the pit is deep. We have plotted in Figure 8 the corrosion rate along the pit wall for the three geometric shapes: deep pit, hemispherical pit and shallow pit.

Figure 8 clearly shows that the corrosion rate is always higher at the mouth of the pit than at the bottom, and this is solely due to the ohmic drop in potential in the cavity. Similarly, the shallower the

pit, the lower the ohmic drop in potential as shown in the studies of Tricoit [28], Mouloudi *et al*. [17] and Oltra *et al.* [29].

The pit shallow according to Figure 8 has a higher corrosion rate than the other pit forms. Therefore, it can be concluded that the evolution of the shallow pit is faster than the hemispherical pit and the deep pit. These results were confirmed by the work of Wang *et al.* [16] who studied the effect of geometric shape on the evolution of pit morphology and found that the shallow pit shape grows faster than the other shapes while the pits keep symmetrical morphology in the evolution process of pitting corrosion.

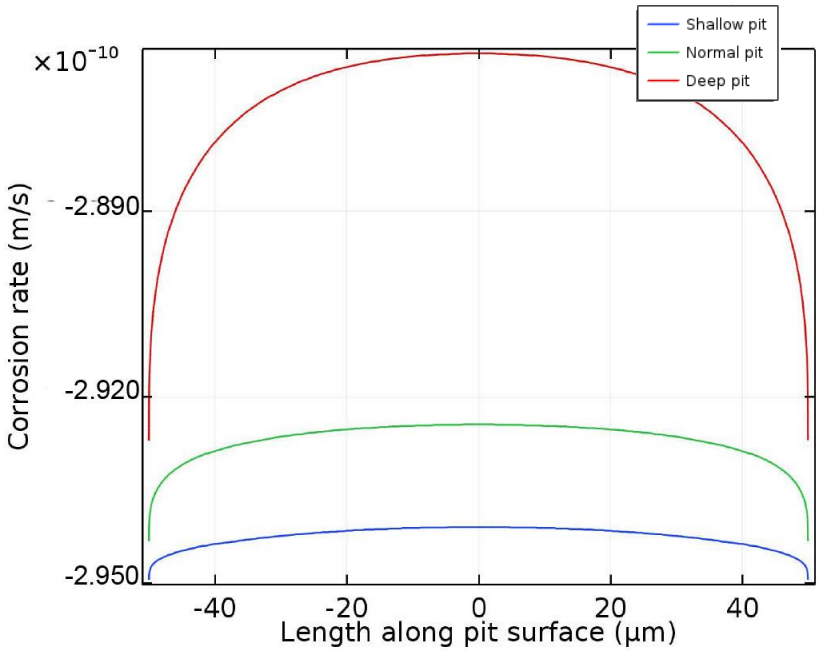

Figure 8. Influence of the pit shape on the corrosion rate along the pit wall.

In summary, the decrease in ion concentration inside the pit leads to a decrease in the current density of the electrolyte, which reduces the ohmic drop and thus accelerates the corrosion of the metal in the pit.

4. CONCLUSION

In the present work, a multi-species reactive transport model of aluminum pitting corrosion in a 1M NaCl aqueous solution has been proposed. This model takes into account both the physicochemical phenomena involving the mass transport processes, the homogeneous chemical reactions in the solution and the electrochemical reactions at the metal/solution interface.

We have studied by numerical simulation based on the finite element method the evolution dynamics of pitting corrosion as well as the effect of the geometrical shape on the local environment of the pit. The main conclusions drawn from the results obtained are the following:

- The concentration of Al^{3+} is higher at the bottom of the pit indicating the dissolution of the metal which favors the hydrolysis reaction and consequently the production of $AlOH^{2+}$ and H+ ions. The accumulation of H^+ ions reduces the pH which leads to an acidic and corrosive environment in the presence of Cl^- ions;

- The geometric pit shape influences the local chemical and electrical environment. The concentration of Al^{3+} accumulates in abundance in the deep pit compared to the hemispherical pit and the shallow pit. Due to the hydrolysis reaction of Al^{3+}, the concentration of H^+ ions is also higher at the bottom of the deep pit compared to the other geometric shapes;

- The current density of the electrolyte is higher in the deep pit due to the high concentration of Al^{3+} and H^+ ions. Thus the chemical environment of the pit has a more pronounced effect on the electrolyte current density;

- The corrosion rate of the shallow pit is higher than other forms of pit, and this is due to the ohmic drop of the low potential which accelerates the corrosion of the metal.

The model developed in this study is able to predict the evolution of aluminum pitting corrosion by integrating electrochemistry and mass transport. Future work will consist in developing this model by taking into account the presence of precipitated phases (oxide films or corrosion products) in order to determine their roles in the transport phenomena and corrosion kinetics.

References

1. Y. Mollapour and E. Poursaeidi, *Engineering Failure Analysis,* 128 (2021) 105589.
2. N. Bensalah, Pitting Corrosion, (2012) IntechOpen, London.
3. S. Salleh and N. P. C. Stevens, *Journal of Engineering and Technology*, 4(1) (2013) 159-169.
4. D. Di Caprio, C. Vautrin-UI, J. Stafiej, J. Saunier, A. Chaussé, D. Féron and J. P. Badiali, *Corros. Sci.*, 53(1) (2011) 418-425.
5. Y. Wang, L. Yin, Y. Jin, J. Pan and C. Leygraf, *J. Electrochem. Soc.*, 164(14) (2017) C1035-C1043.
6. E. McCafferty, *Corros. Sci.,* 45(7) (2003) 1421–1438.
7. Z. Szklarska-Smialowska, *Corros. Sci.,* 53(1) (1999) 1743-1767.
8. R. Duddu, *Comput. Mech.,* 54(3) (2014) 613-627.
9. S. M. Sharland and P. W.+ Tasker, *Corros. Sci.,* 26(6) (1988) 603-620.
10. R. Oltra, A. Zimmer, C. Sorriano, F. Rechou, C. Borkowski and O. Néel, *Electrochim. Acta,* 56(20) (2011) 7038– 7044.
11. J. Xiao and S. Chaudhuri, *Electrochim. Acta*, 56(16) (2011) 5630–5641.
12. S. Salleh and N. P. C. Stevens, *Journal of Mechanical Engineering and Technology,* 4(1) (2012) 1-14.
13. S. Salleh and N. P. C. Stevens, *ARPN Journal of Engineering and Applied Sciences,* 13(1) (2018) 134-139.
14. O. Guseva, J. A. DeRose and P. Schmutz, *Electrochim. Acta*, 88 (2013) 821– 831.
15. O. Guseva, P. Schmutz, T. Suter and O. Von Trzebiatowski, *Electrochim. Acta*, 54 (19) (2009) 4514–4524.
16. K. Wang, C. Li, Y. Li, J. Lu, Y. Wang and X. Luo, *J. Electrochem. Soc.,* 167(1) (2020) 013505.
17. M. Mouloudi, R. Radouani, M. Essahli, M. Chafi and M. Chhiba, *Int. J. Electrochem. Sci.,* 16 (2021) 21119.
18. A. TURNBULL, *Br. Corros. J.,* 28(4) (1993) 297-308.

19. A. F. Chadwick, J. A .Stewart, R. A. Enrique, S. Du and K. Thornton, *J. Electrochem. Soc.,* 165(10) (2018) C633-C646.
20. V. A. Nguyen and R. C. Newman, *Corros. Sci.,* 186 (2021) 109461.
21. S. M. Sharland, C. P. Jackson and A. J. Diver, *Corros. Sci.*, 29(9) (1989) 1149-1166.
22. Q. Li, J. O. Jensen and N. Bjerrum, *Encyclopedia of Electrochemical Power Sources*, Elsevier, (2009) pp. 695-708.
23. J. Jung, S. Oh and H. Kwon, *Mater. Corros.*, 72(3) (2021) 557-563.
24. J. Peng, G. Ji, Z. Shi and X. Wang, *ACS Omega*, 6 (22) (2021) 14504−14517.
25. Y. H. Lee, Z. Takehara and S. Yoshizawa, *Corros. Sci.,* 21(5) (1981) 391-397.
26. Y. Yuan, L. Li, C. Wang and Y. Zhu, *Electrochemica Communications,* 12(12) (2010) 1804-1807.
27. N. Sato, *Corros. Sci.,* 37(12) (1995) 1947-1967.
28. S. Tricoit, Modeling and numerical simulation of iron pitting corrosion propagation in chloride media, Thesis, University of Burgundy, UFR Sciences et Techniques, The laboratory Interdisciplinaire Carnot de Bourgogne (2012), Andra, France, Available at : https://tel.archives-ouvertes.fr/tel-01083061/document.
29. R. Oltra, J. L. Mousson, B. Vuillemin and R. Cottis, *CORROSION 2004*, (2004) OnePetro, New Orleans, Louisiana.